The impact of tidal energy extraction is estuaries: analysis of the influence of channel geometry.

Miriam Garcia-Oliva[☆], Slobodan Djordjevic, Gavin R. Tabor

College of Engineering, Mathematics and Physical Sciences
University of Exeter, North Park Road, Exeter, EX4 4QF, United kingdom

Abstract

Macro-tidal estuaries in the UK not only have a high tidal range but also present strong currents in some cases, where tidal farms could be used for energy extraction but not forgetting about the associated environmental impacts beforehand.

The purpose of this study is to delimit the influence that the geometry of the channel could have over the impact of a tidal farm deployed in the estuary. A hydrodynamic model (Mike21) has been used to create several cases of idealised estuaries with dimensions based on a group of locations suitable for tidal energy extraction in the UK. The maximum changes in low and high water levels with the tidal farm have been identified for each case and located within the estuary. The changes in the time for the low and high tides in a point inside the estuary have also been analysed. The effect of the drag coefficient of the turbines over the changes in water levels has been addressed as well.

As a conclusion, it can be noted that the maximum changes in water levels due to the farm range from the order of mm to a few dm and the locations of these changes are strongly dependent on the geometry of each case. In addition, the effect is generally more noticeable in the increase of low water levels and the decrease of high water levels than vice-versa. This would be associated with the loss of intertidal areas and the reduction of flood risk levels. In terms of the changes in the time of low and high water levels, the effects of the farm are negligible in all cases. Finally, the use of a higher drag coefficient seems to increase the changes on water levels.

Keywords: Tidal farm, Hydrodynamic impact, Estuaries, Idealised model, Sensitivity analysis, Finite volume method

1. Introduction

Tides are a constant and predictable source of energy. This fact represents an advantage over other renewable energy sources which are intermittent and involve a higher level of uncertainty in the estimation of the available resource. Therefore, tidal technologies could be used in a complementary way with other renewable schemes in order to cover the electricity demand in a more efficient way. Additionally, tidal energy can be considered as an autonomous solution for less accessible locations. As indicated in the report by [1], the use of marine renewables can provide lower costs and reliability in the supply of far-peripheral areas and islands.

There is a high availability of tidal energy resource in the UK. The strongest tidal currents usually happen in offshore locations while the highest tidal ranges are mostly observed in estuarine areas, as can be seen from [2]. Nevertheless, it should be mentioned that some estuaries also show tidal currents over 1 m/s, reaching spring values over 2 m/s at specific locations like the Severn estuary [3]. Thus, the use of tidal schemes in such estuaries could benefit from the combination of tidal stream and ranges.

On the other hand, environmental aspects related to the use of tidal technologies must be considered carefully in estuaries, which are typically protected areas for the conservation of nature. An effect of tidal energy extraction that can be analysed more immediately is the change in the hydrodynamic behaviour of the estuary, which will affect other environmental aspects, such as sediment transport, water quality, flood risk, intertidal habitats, etc.

Previous studies have been carried out in relation to the assessment of environmental impacts of tidal energy

[☆]Corresponding author. *Email address:* mg391@exeter.ac.uk (Miriam Garcia)

schemes in estuaries. Some of them are related to the deployment of tidal barrages and lagoons [4], while others analysed the use of tidal stream turbines [5], [6]. Most of these studies apply numerical models to describe the hydrodynamics of a certain location with the level of detail given by the use of the real bathymetry and boundary conditions. Analytical models have also been used extensively to analyse the effects that energy extraction could have on the hydro-environmental conditions and the remaining available power in channels. Some examples can be found in ([7], [8], [9]). These models offer a reduced computational demand and can give an estimation of the desired results when a high degree of accuracy is not required. However, it must be highlighted that they are only valid under certain specific circumstances.

Accordingly, the results from the aforementioned models depend on intrinsic parameters, such as the geometry or bathymetry of the basin, the boundary conditions and the bed roughness, amongst others. In this sense, the study by [10] stated that the sensitivity of a simple channel to energy extraction is related to water depth, length, width and the nature of boundary roughness. Based on this idea, the aim of this study is to delimit the effect of the geometry over the impact that tidal farms have when they are installed in estuaries. This impact is here mainly related to the water levels because they affect aspects such as flood risk levels and changes in intertidal habitats, which are important issues in estuaries.

This study considers the deployment of block tidal farms, which occupy partially the width of the estuary, leaving space for other activities. It has also been considered the use of turbines supported by floating structures, which adapt to the tidal levels and can be moved to different positions within the estuary if necessary.

For the purpose of this research, idealised models have been used to represent different geometries based on existing estuaries in the UK suitable for tidal energy extraction. The same tidal farm and conditions have been used in all cases and a sensitivity analysis has been performed over the variation of the geometrical parameters in the idealised models. Idealised models benefit from a reduction in computational demand, which allows to test numerous scenarios, and an easier identification of physical trends [11]. Regarding previous studies about the application of idealised models to estuaries two main groups can be found: the projects related to the estuarine morphodynamics ([11], [12], [13]), and the more recent research about the effects of tidal energy extraction in estuaries ([14], [15]). Regarding the second group, an example closer to this study can be found in the thesis by [16], where a group of generic coastal geometries, including estuaries, are used to identify the effects of a tidal fence.

This paper is organised at follows. Initially, the methodology used in order to select the estuaries covered in this study, classify their geometries and create the idealised models is presented. The next section describes the numerical model used, the parameters involved and the design of the tidal farms included in the models. Finally, the results are shown and discussed in order to extract the main conclusions about the effect that geometry has on the impact of tidal farms in estuaries.

2. Materials and Methods

2.1. Estuaries Classification

For the purpose of this study, the main estuaries in the UK with a high resource of tidal energy were first identified based on the report carried out by [2]. The report differentiates between the locations with a high tidal range or tidal stream energy resource (please see Fig. 1). It can be seen that most of the tidal stream resources are generally located in offshore areas, except for the Bristol Channel, while the tidal range resources appear to be only related to estuaries. It should be mentioned that schemes such as barrages or lagoons are not the only options for some of the locations with high tidal range. According to the information provided by the Atlas of UK Marine Renewable Energy [17], velocities frequently show values over 1m/s in some locations, reaching peak flows up to 2 m/s in a few cases . This fact allows them to be considered as potential locations for the installation of tidal in-stream turbines, which are the focus of this project.

In order to complete the list of estuaries suitable for tidal energy extraction, other macro-tidal estuaries were identified through the information provided by the estuary data base [18] and the peak flows in these estuaries were analysed by means of the Atlas of UK Marine Renewables [17]. In some estuaries where the Atlas did not have coverage, some of these details were obtained from the existing literature ([19], [20], [21], [22], [23], [24]). Only the estuaries with peak flows above 1 m/s have been considered for this study (Please see Table 1)

2.2. Geometrical Characterisation of the Estuaries

Following, the main dimensions of the estuaries selected for this study were obtained from different sources, such as the estuary guide [18] and [25], [26], [27], [28], [29]. These values can be seen in Table 2.

The study by [29] presented a formula to relate the mean depth with the depth at the mouth of the estuary:

$$D_{mouth} = 1.8 D_{mean} \tag{1}$$

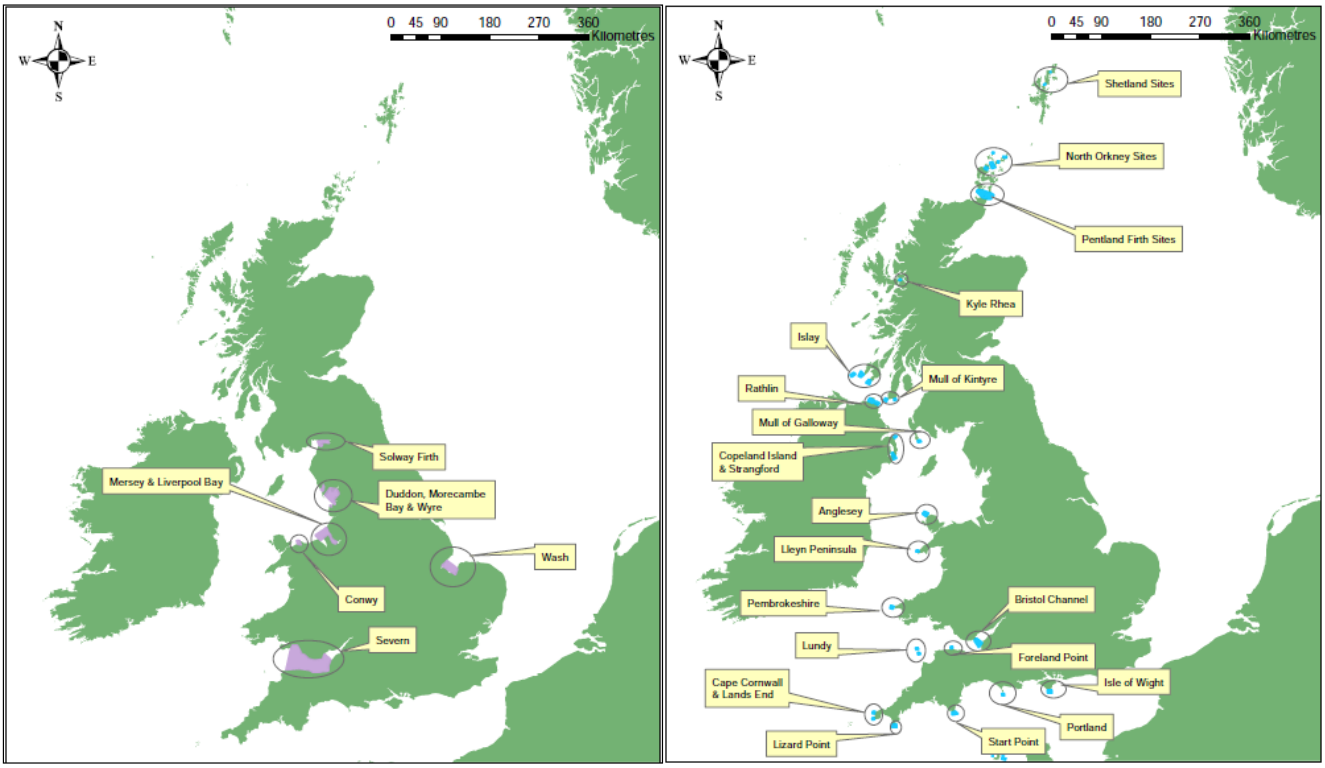

Figure 1: Tidal range (left) and stream (right) resource locations (source: UK Tidal Resource Review V5 Sustainable Development Commission)

Estuary	Tidal range (m)	Current speed (m/s)
Severn	13	2
Thames	6.5	1
Ribble	7.9	1.5
Duddon	8.1	1
Morecambe Bay	8.4	1
Mersey	8.9	2
The Wash	6.5	1
Humber	7.2	2
Solway Firth	8.4	2

Table 1: Estuaries included in this study: maximum tidal range and approximate maximum limit of the current speed (which can be sometimes exceeded)

Estuary	Length (km)	Width at mouth (km)	Width at head (m)	Depth at mouth (m)	Depth at head (m)
Severn	111.2	6836	200	63.54	7.06
Thames	82.5	2191	90	43.38	4.82
Ribble	28.4	3129	-	12.78	0.98
Duddon	22.6	2094	50	8.82	0.92
Morecambe Bay	40.3	13493	-	8.28	0.88
Mersey	45.6	1706	150	7.92	3.16
The Wash	90.2	19360	50	28.44	2.32
Humber	144.7	7366	500	20.88	2.1
Solway Firth	46.3	7091	80	14.94	1.72

Table 2: Main dimensions of the estuaries considered in this study. (- : information not available)

It has been used to determine the values of the depth at the mouth in Table 2 and at the head of the estuaries where this information was not available.

2.3. Idealised Cases

The values shown in Table 2, were analysed in order to define three ranges that could be named as small, medium and large dimensions, as can be seen from Fig. 3

The variation of the width and the depth over the length of the estuary has been calculated as:

$$\Delta W = \frac{W_H}{W_M L} \tag{2}$$

$$\Delta D = \frac{D_H}{D_M L} \tag{3}$$

being the subscripts H or M related to the head and the mouth of the estuary, respectively, and L the total length of the estuary.

Based on the ranges shown in Table 3, fifteen cases (case 1.a to case 3.iii) with different geometry where created by varying one of the parameters and fixing the rest. Two more cases were included in order to provide a more detailed analysis of the longitudinal depth variation because the results, as it will be explained in the next section of this document, showed that this parameter had a higher influence than others.

The cross section of the channel is another aspect that needs to be considered. Therefore, in order to account for three different sizes of the lateral slopes in the channel walls with the same cross sectional area, other six cases (case 4.a to case 5.c) were defined in which either the width or the depth were fixed. This would lead to three kinds of shape for the cross section, that is, rectangular, trapezoidal or triangular. Finally, based on the triangular cross section, three more cases (case 6.a to case 6.c) were defined in order to represent different lateral slopes with the same area. The lateral slope in Figure 5 is defined as the ratio between horizontal and vertical dimensions, that is, a smaller slope means that the sides of the cross section are closer to the vertical shape. All the geometrical parameters for the cases used in the sensitivity analysis can be found in Table 4.

2.4. Numerical Model

Mike 21 by DHI was used in this study to represent the hydrodynamic conditions of the estuaries and the influence of a tidal farm. It uses a 2-dimensional (2D) numerical model based on the finite volume method to solve the Reynolds averaged Navier-Stokes equations. A rectangular flexible mesh was used in this study for the spatial discretisation of the governing equations, which can follow a first or a second order scheme. An approximate Riemann solver is used for the calculation of the convective fluxes at the cell interface using linear gradient reconstruction techniques which provide second order accuracy. Numerical oscillations are avoided by means of a TVD slope limiter. For the time integration, a low or higher order method can be applied. In order to provide stability, the time step is varied according to the restriction that the Courant-Friedrich-Levy (CFL) number is less than 1. [30], [31]. The governing equations are the continuity and the momentum equations (4), (5),

Length (km)	Small	0 - 50
	Medium	50 - 100
	Large	100 - 150
Width at the mouth (m)	Small	0 - 7000
	Medium	7000-14000
	Large	14000-21000
Depth at the mouth (m)	Small	0-20
	Medium	20-40
	Large	40-60
Width variation (1/km)	Small	0-0.0007
	Medium	0.0007-0.0014
	Large	0.0014-0.0021
Depth variation (1/km)	Small	0-0.0016
	Medium	0.0016-0.0032
	Large	0.0032-0.0048

Table 3: Ranges of parameters, based on the estuaries analysed in this study

(6).

$$\frac{\partial h}{\partial t} + \frac{\partial h}{\overline{u}}\partial x + \frac{\partial h}{\overline{u}}\partial y = hS \tag{4}$$

$$\begin{aligned}\frac{\partial h\overline{u}}{\partial t} + \frac{\partial h\overline{u}^2}{\partial x} + \frac{\partial h\overline{uv}}{\partial y} &= f\overline{v}h - gh\frac{\partial \eta}{\partial x} - \frac{h}{\rho_o}\frac{\partial p_a}{\partial x} \\ -\frac{gh^2}{2\rho_o}\frac{\partial \rho}{\partial x} + \frac{\tau_{sx}}{\rho_o} - \frac{\tau_{bx}}{\rho_o} - \frac{1}{\rho_o}&\left(\frac{\partial s_{xx}}{\partial x} + \frac{\partial s_{xy}}{\partial y}\right) \\ +\frac{\partial}{\partial x}\left(hT_{xx}\right) + \frac{\partial}{\partial y}&\left(hT_{xy}\right) + hu_sS\end{aligned} \tag{5}$$

$$\begin{aligned}\frac{\partial h\overline{v}}{\partial t} + \frac{\partial h\overline{uv}}{\partial x} + \frac{\partial h\overline{v}^2}{\partial y} &= f\overline{u}h - gh\frac{\partial \eta}{\partial y} - \frac{h}{\rho_o}\frac{\partial p_a}{\partial y} \\ -\frac{gh^2}{2\rho_o}\frac{\partial \rho}{\partial y} + \frac{\tau_{sy}}{\rho_o} - \frac{\tau_{by}}{\rho_o} - \frac{1}{\rho_o}&\left(\frac{\partial s_{yx}}{\partial x} + \frac{\partial s_{yy}}{\partial y}\right) \\ +\frac{\partial}{\partial x}\left(hT_{xy}\right) + \frac{\partial}{\partial y}&\left(hT_{yy}\right) + hv_sS\end{aligned} \tag{6}$$

Where η = bed elevation, h = water depth, u and v = velocity components in x and y directions, respectively, g = gravitational acceleration, ρ_o = reference density of the water, s_{ij} = components of the radiation stress tensor, p_a = atmospheric pressure, τ_{bx}, τ_{by} = bottom stresses, τ_{sx}, τ_{sy} = wind or ice stresses, T_{ij} the lateral stresses including viscous friction, turbulent friction and differential advection, S the discharge from sources and u_s, v_s the velocity components of the water discharged into ambient.

The model also includes the equations for temperature, salinity and density and includes a turbulence model. A more detailed description of the model can be found in [30], [31].

Representation of turbines

Based on the idea that structures are generally smaller than the extent of the mesh element, turbines are modelled as sub-grid structures using basic equations to calculate the overall impact in the cell, instead of performing detailed modelling. The effect of turbines is included in the governing equations as an additional shear stress term from the drag force imposed to the flow, with axial and transverse components as follows:

$$F_d = \frac{1}{2}\rho\alpha C_d A_e v^2 \tag{7}$$

$$F_l = \frac{1}{2}\rho\alpha C_l A_e v^2 \tag{8}$$

Where α is a correction factor, C_d and C_l are the drag and lift coefficients respectively, A_e is the effective area of the turbine and v is the velocity of the flow incident into the turbine or the current value in the element wherein the turbine is positioned. This value is influenced by the former time steps in the calculation and is affected by the presence of the turbine but it is not to be interpreted as the current speed through the turbine. [30]

2.5. Application to the idealised estuaries

The geometries, previously described in subsection 2.3- Idealised Cases, were used to generate a mesh, inter-

Case	Length (km)	Width at mouth (m)	Width variation (/km)	Depth at mouth (m)	Depth variation (/km)	Lateral slope (1/m)	Cross section
1.a	**25**	10500	0	30	1.000	0	Rectangular
1.b	**75**	10500	0	30	1.000	0	Rectangular
1.c	**125**	10500	0	30	1.000	0	Rectangular
2.a	75	**3500**	0	30	1.000	0	Rectangular
2.b	75	**10500**	0	30	1.000	0	Rectangular
2.c	75	**17500**	0	30	1.000	0	Rectangular
2.i	75	10500	**0.0018**	30	1.000	0	Rectangular
2.ii	75	10500	**0.0011**	30	1.000	0	Rectangular
2.iii	75	10500	**0.0004**	30	1.000	0	Rectangular
3.a	75	10500	0	**10**	1.000	0	Rectangular
3.b	75	10500	0	**30**	1.000	0	Rectangular
3.c	75	10500	0	**50**	1.000	0	Rectangular
3.i	75	10500	0	30	**0.004**	0	Rectangular
3.i-ii	75	10500	0	30	**0.0032**	0	Rectangular
3.ii	75	10500	0	30	**0.0024**	0	Rectangular
3.ii-iii	75	10500	0	30	**0.0016**	0	Rectangular
3.iii	75	10500	0	30	**0.0008**	0	Rectangular
4.a	75	10500	0	**60**	1.000	**87.5**	Triangular
4.b	75	10500	0	**40**	1.000	**65.625**	Trapezoidal
4.c	75	10500	0	**30**	1.000	**0**	Rectangular
5.a	75	**21000**	0	30	1.000	**350**	Triangular
5.b	75	**15750**	0	30	1.000	**175**	Trapezoidal
5.c	75	**10500**	0	30	1.000	**0**	Rectangular
6.a	75	**21000**	0	**30**	1.000	**350**	Triangular
6.b	75	**16601**	0	**38**	1.000	**218.75**	Trapezoidal
6.c	75	**10500**	0	**60**	1.000	**87.5**	Rectangular

Table 4: Geometrical dimensions for the different cases used in the study (yellow indicates the parameters that are not fixed on each case).

polated over the bathymetry, to be used as a domain for the models. The maximum size of the cells was set up to $1km^2$. The simulation period covered 6 days, with a time step of 900 seconds. Regarding the stability of the models, the Courant-Friedrich-Levy (CFL) number was limited to a maximum value of 0.8.

A flood and dry function was activated in all the models to remove the cells from the calculation when the depth is very small (dry elements). The parameters involved in the flood and dry function consisted of a drying depth of 0.005 m, a flooding depth of 0.05 m and a wetting depth of 0.1m.

A constant bed roughness was used over the domain being the inverse of the Manning coefficient equal to 40 for all the models. Regarding the turbulence parameters, a Smagorinskys coefficient of 0.28 was used as a constant value in the domain. The Coriolis force was not included in the calculations.

At the open sea boundary a Flather condition was used consisting of a zero velocity condition and the tidal curve

for the water levels. The tidal levels were approximated as a cosine function of the M2 tide with amplitude of 9 m. Nevertheless, the river discharges were not included in the models for simplicity. It was important to use the same conditions for all the models in order to be able to compare the results between them.

Tidal farm

The Momentum Reversal Lift turbine (MRL), developed by Aquascientific Ltd. in collaboration with the University of Exeter, has been used in this study. It presents some advantages in this case when compared to other designs, such as the adaptability of the floating support structure to the varying water levels in macrotidal estuaries and the suitability of its dimensions to be used in shallower areas. It is a horizontal cross-flow turbine with three blades that rotate around the axis of the turbine and also around their individual axis. More information can be found in the study by [32].

A tidal farm consisting of 3025 turbines organised in 55 rows by 55 columns following a parallel layout was installed in the central area of each model. The same tidal farm was used in every case because it allows to compare the effect of the geometry on the results. The maximum installed capacity of the farm was approximately 1.1 GW, calculated based on peak current speed of 2m/s and a power coefficient of 0.5, taken from the experimental results in [32]. Each turbine had a diameter of 6 m and a length of 30 m, based on an aspect ratio of 1:5 for the MRL turbine. The turbine diameter covers 70 % of the water column for the minimum depth (8.6 m), which has been taken from the results of the model without turbines in the shallowest case. The lateral spacing between turbines was 0.5 times the turbine length and the longitudinal spacing between two rows of turbines was 10 times the turbine diameter. The longitudinal spacing was based on the work by [33].

For the definition of the turbines in Mike 21, an equivalent diameter had to be defined because it is only referred to axial flow designs. Thus, a value of 15.14 m, which provides the same frontal area as the rectangle of 6x30 m in the real turbines, was used in the calculations. For the representation of the effect of the turbines in the flow, a drag coefficient of 0.9 has been chosen from the information provided by [34], due to the lack of experimental data. The design of the Gorlovs crossflow turbine is closer to the MRL turbine than the axial ones. For simplicity, a fixed drag coefficient and no lift coefficient were used and therefore, the correction factor α from equations (7) and (8) was set equal to 1.

In order to assess the effect of the drag coefficient in the results, four more cases were used based on case 1b with different drag coefficients (1.0, 2.0, 5.0 and 10.0).

3. Results

The results of the water levels in the model domain during the period of the simulation were obtained for each case in the situation with and without the tidal farm. The results for the last half of the simulation were extracted, in order to remove the warm up period. The statistical analysis tool in Mike21 was applied to calculate the maximum and minimum values of the water levels at each location of the domain, thus being related to the high and low tides. Following, the difference between the water levels for the high and low tide in the situations without turbines and with the tidal farm was calculated for each case. The differences give an idea about the effect that the tidal farm can have on every channel geometry. Fig. 2 shows an example of these results for case 1b. The results of the differences between water levels were analysed to determine the maximum increase and decrease in the water levels over the domain, which are included in Table 5.

The results for the cases with longitudinal depth variation (cases 3.i to 3.iii) were used to plot a graph (please see Fig. 3) where it can be seen that the most important effect appears in the increase of low tide levels and it follows quite a linear behaviour.

The locations where the maximum increase and decrease happen both for the low and high tides were also identified by using the scheme from Fig. 4 and summarised for each case in Table 6.

The time series of the water levels over the last half of the simulation were also obtained in a point located at the longitudinal axis of the estuary and one quarter of the estuary length from the head. These results shown that there was not any appreciable change in time for the high and low tides with the presence of the tidal farm in any case. As an example, the results for case 1.b have been included in Fig. 5.

The results for the cases with a different drag coefficient were analysed in the same way as the rest of the cases in order to find the maximum increase and decrease in the low and high tide levels due to the effect of the tidal farm, as can be seen in Table 7.

These results have been plotted in Fig. 6.

4. Discussion of the Results

When analysing the results in terms of each parameter, it can be seen that, in general:

- Length has inverse effects than width or depth.

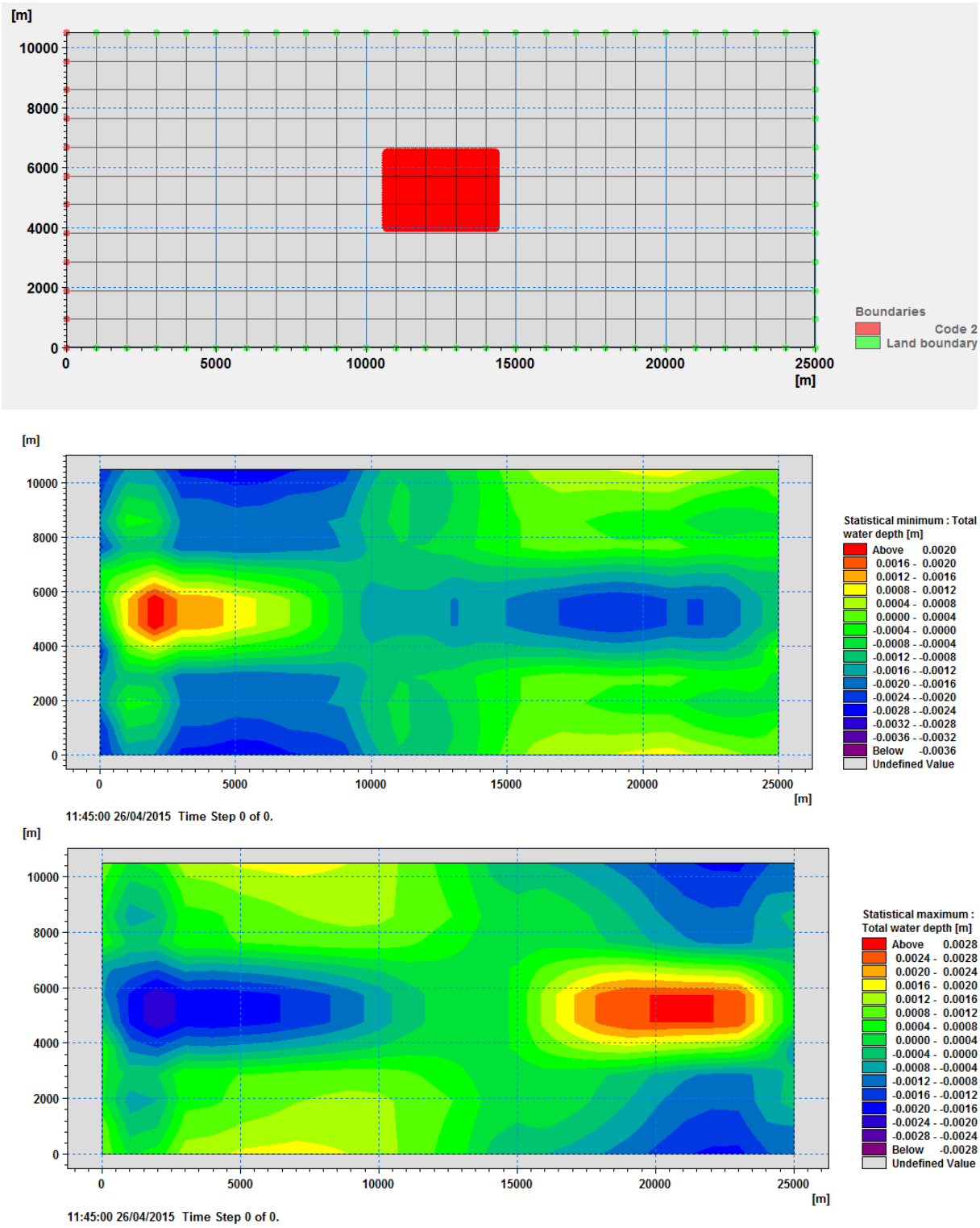

Figure 2: Case 1a / Upper image: Computational domain and tidal farm; Central image: Difference in high water levels with the tidal farm ; Lower image: Difference in low water levels with the farm.

Case	Difference low levels (m)		Difference high levels (m)	
	Max. increase	Max. decrease	Max. increase	Max. decrease
1.a	0.003	0.004	0.003	0.003
1.b	0.026	-	-	0.019
1.c	0.038	0.011	0.016	0.046
2.a	0.133	-	-	0.124
2.b	0.026	-	-	0.019
2.c	0.016	-	-	0.013
2.i	0.017	-	0.006	0.006
2.ii	0.015	-	0.005	0.005
2.iii	0.013	0.002	0.004	0.005
3.a	0.052	0.020	0.080	0.051
3.b	0.026	-	-	0.019
3.c	0.007	-	0.002	0.004
3.i	0.102	0.007	-	0.076
3.i-ii	0.122	0.008	-	0.084
3.ii	0.142	0.007	-	0.089
3.ii-iii	0.160	0.006	-	0.090
3.iii	0.178	0.005	0.012	0.091
4.a	0.054	0.002	-	0.040
4.b	0.043	0.003	-	0.031
4.c	0.026	-	-	0.019
5.a	0.077	0.033	0.046	0.063
5.b	0.076	0.014	-	0.200
5.c	0.026	-	-	0.019
6.a	0.077	0.033	0.046	0.063
6.b	0.072	0.023	-	0.142
6.c	0.054	0.002	-	0.040

Table 5: Maximum increase and decrease of water levels for the low and high tides over the model domain with the inclusion of a tidal farm.

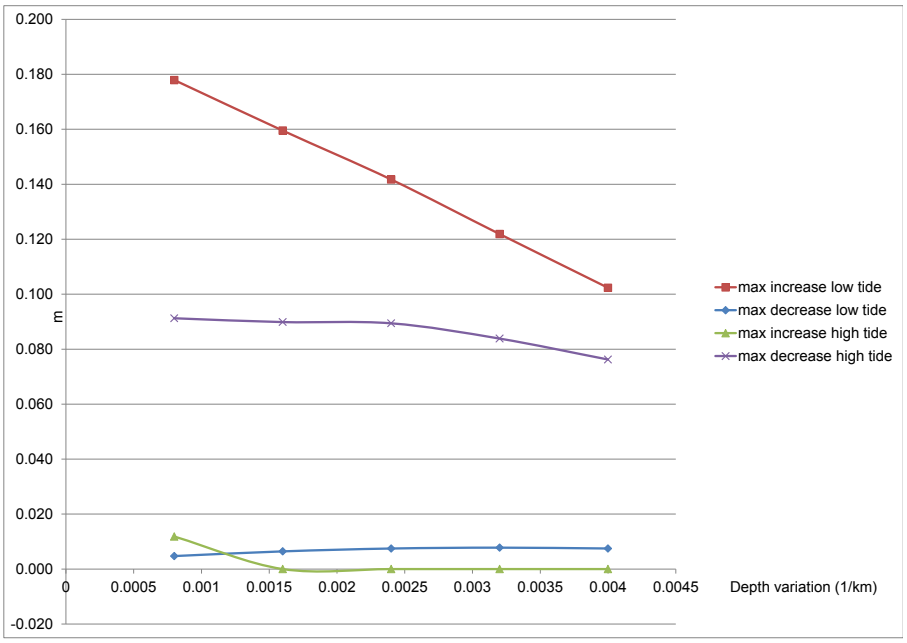

Figure 3: Maximum increase and decrease of low and high tide levels for the cases with longitudinal depth variation

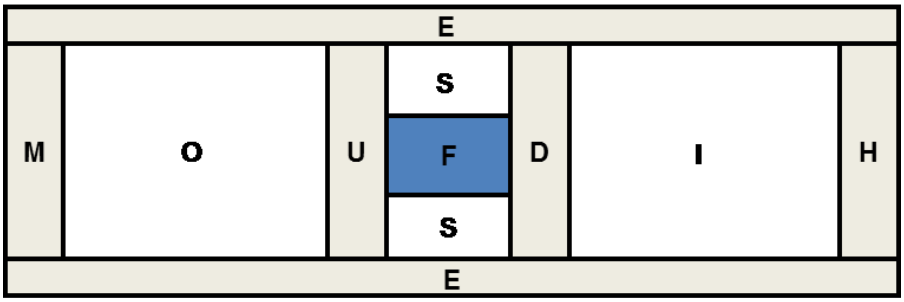

Figure 4: Scheme of the estuary (M: mouth of the estuary; O: outer area; U: area upstream the farm; F: tidal farm: S: sides of the farm; D: area downstream the farm; I: inner area; H: head of the estuary; E: edges of the estuary)

Case	Difference low levels / locations		Difference high levels / locations	
	Max. increase	Max. decrease	Max. increase	Max. decrease
1.a	O	I	I	O
1.b	D	-	-	S
1.c	I/U/S/D	O	O	I/U/S/D
2.a	O	-	-	I
2.b	D	-	-	I
2.c	I	-	-	S
2.i	S	-	I	S
2.ii	O/S	-	I	S
2.iii	O/S	I	I/S	S
3.a	I/D	O/U	O	U/S/D
3.b	D	-	-	S
3.c	O/S	-	O/U	S/D
3.i	I/D	O	-	O
3.i-ii	O	D	-	O
3.ii	I/D	O	-	O/S
3.ii-iii	M/H	D	-	H
3.iii	I/D	O	O	S/H
4.a	U/S/D	E	-	O
4.b	I/D	O/S	-	O
4.c	D	-	-	S
5.a	I	M	M	U
5.b	I	M	-	M
5.c	D	-	-	S
6.a	I	M	M	U
6.b	I/D	M	-	M
6.c	U/S/D	E	-	O

Table 6: Locations of the maximum increase and decrease of high and low tide levels within the estuary. (Please see Figure 9 for the meaning of the capital letters).

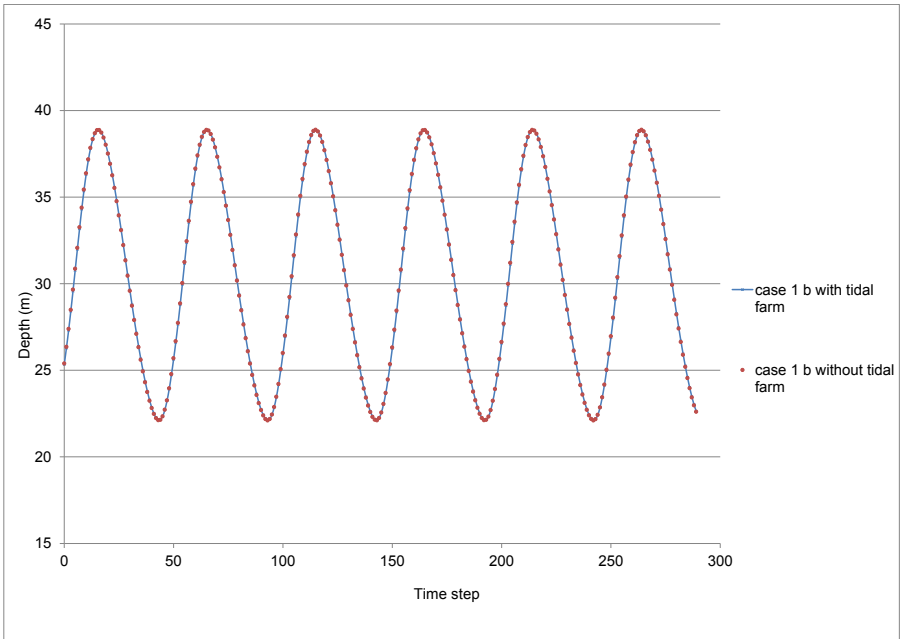

Figure 5: Water levels in the situations with and without the tidal farm over the last three days of the simulation at a point with coordinates (3L/4, W/2), being L and W the estuary length and width, respectively

Case	Difference low levels (m)		Difference high levels (m)	
	Max. increase	Max. decrease	Max. increase	Max. decrease
1.b Cd 0.9	0.026	-	-	0.019
1b Cd 1.0	0.027	-	-	0.020
1b Cd 2.0	0.034	-	-	0.029
1b Cd 5.0	0.044	-	0.010	0.042
1b Cd 10.0	0.056	-	0.020	0.053

Table 7: Maximum increase and decrease of low and high tide levels with a tidal farm with different drag coefficient for the turbines in case 1b.

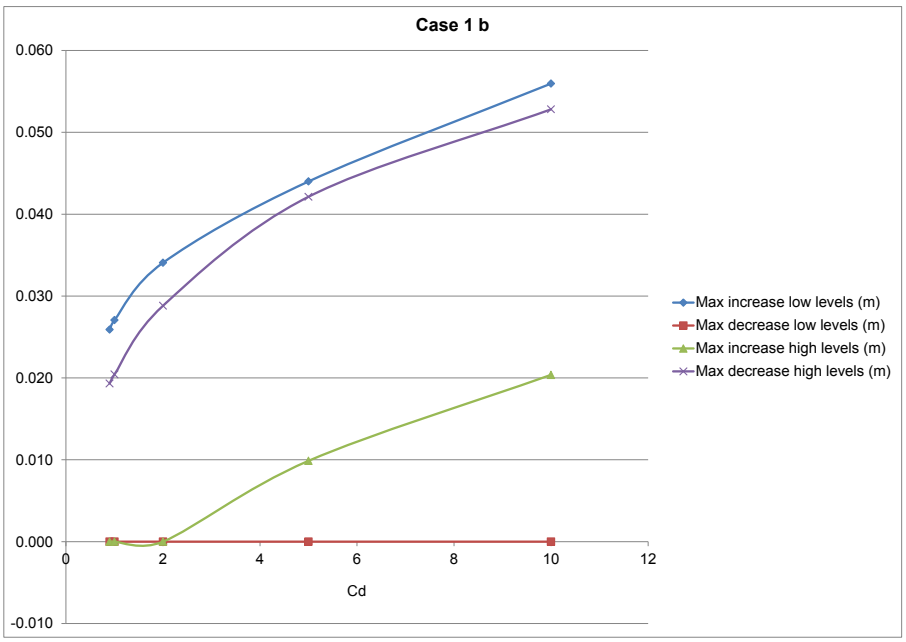

Figure 6: Maximum increase and decrease of low and high tide levels in case 1 b with different drag coefficients of the turbines in the tidal farm.

- Longitudinal width variation has smaller effects than the equivalent case with constant width (case 2b).
- Longitudinal depth variation has a stronger overall effect compared to the equivalent case with constant depth (case 3b).
- A more horizontal lateral slope has more influence both over low and high tidal levels than a more vertical one.

Focusing on the results separately for the increase and decrease of low and high tidal levels, it can be noted that:

- Regarding the maximum increase in low tidal levels, the most relevant effect appears in the inner area and downstream the farm in case 3iii, being in the order of 18 cm. Apart from the longitudinal variation cases, case 2a, which represents the narrowest case in the study, also shows a significant increase, reaching up to 13 cm in the outer area of the estuary. Basically, longitudinal depth variation and width have stronger effects than the other parameters over the increase of low tidal levels, which can be associated to the permanent submersion of intertidal areas.
- In relation to the maximum decrease of low tidal levels, the highest value (3 cm) happens in the mouth of the estuary in cases 5a and 6a, with the same triangular cross-section, which represent a more horizontal lateral slope. While in several of the other cases the value of the decrease is almost imperceptible. The decrease of low tidal levels could have an associated increase of the extension of intertidal areas.
- When comparing the results for the maximum increase of high tidal levels, which have a consequence on the increase of flood risk levels and the extension of intertidal areas, the overall highest value (8 cm) appears in the outer area of case 3a, which is the shallowest case. On the other hand, the triangular section with a more horizontal lateral slope also has a higher effect (approximately 5 cm in the mouth of the estuary). The rest of the cases do not show important changes in this sense.
- In reference to the maximum decrease over the high tidal levels, case 5b reaches 20 cm in the mouth of the estuary (which is the absolute maximum change in all cases). Case 6b also shows a significant maximum decrease also in the mouth of the estuary (approximately 14 cm). On the other hand, the width of the estuary seems to have some impact, being the effect higher at the inner part in case 2a (narrowest case). The decrease of high tidal levels has an effect on the decrease of intertidal areas, which change

into permanently dry areas.

Some of the locations where the highest changes appear have been commented in the previous paragraph but there are also other ideas which can be extracted from 6:

- In general, when one of the parameters (depth, width or length without longitudinal variation) is increased, the maximum effects seem to move to different parts of the estuary. For example, in case 1c the maximum increase of low tidal levels and decrease of high tidal levels move from the inner and outer part respectively to different locations including both sides of the tidal farm.
- In cases with a longitudinal variation of the width and depth, maximum changes usually happen in areas different to the equivalent case with a constant depth or width over the length.
- Counting the number of times in Fig. 6 that each kind of location from Fig. 4 registers a maximum change it can be seen that most of these changes happen at both sides of the farm followed by the outer part and less frequently in the inner part of the estuary. In the cases with triangular and trapezoidal cross sections is significant the location of these effects in the mouth of the estuary.

  Changes in time for low-high tides

  In terms of the change of the time for low and high water levels, from the time series extracted at a point at L/4 of the estuary head, it can be mentioned that there is no remarkable change and the highest and lowest levels at that point happen during the same time step with or without the tidal farm for all cases.

  Influence of the drag coefficient of the turbines

  From the analysis of the results in the cases with an increased drag coefficient, it seems that the maximum increase in low levels and decrease in high levels follow a similar trend (please see Fig. 6) and there is not noticeable decrease in low levels for all cases.

5. Conclusion

From the results included in the previous section, it can be concluded that:

- In general, when comparing all the geometries, the effect of the farm would be higher in terms of permanently submerging the intertidal areas (increase in low tidal levels) rather than increasing the extension of intertidal areas (decrease of low tidal levels).
- It could be also mentioned that, with the inclusion of the tidal farm, the decrease in high tidal levels happens to be more relevant than the increase. Therefore, it would mean that the net effect over flood risk could be positive, while, on the other hand, intertidal areas could become permanently dry areas.
- The locations of the maximum changes in low and high water levels happening due to the influence of the tidal farm are strongly dependent on the geometry.
- There are negligible effects for all the cases in changes to the time of high/low tides with the farm.
- There is an increase of the effects in general with a higher drag coefficient although the decrease of low tide levels continue being negligible for all cases with a different drag coefficient in case 1b.

6. Future Research

Future studies may be done by using a similar methodology based on idealised models in order to assess the effect that different configurations and locations of tidal farms or other tidal technologies could have on the environmental aspects of estuaries. The use of different drag coefficients rather than the same fixed coefficient for the turbines in the tidal farm is another issue that needs to be addressed.

Finally, idealised models could be used in the future in order to integrate results from undergoing studies on the optimisation of tidal farms and become a tool to find the configuration of turbines and the combination of drag coefficients which covers both the objectives of maximum energy extraction and minimum environmental impact.

Acknowledgement

This research was conducted as part of the Optimal Design of Very Large Tidal Stream Farms: for Shallow Estuarine Applications project commissioned

and funded by the UK Engineering and Physical Sciences Research Council (EPSRC) - (EP/J010138/1). The authors would also like to acknowledge the support and software licence provided by DHI.

Bibliography

[1] P. Garzon, Y. Rabuteau, K. Stanley, Civil society involvement and social acceptability of marine energy projects.-best practices of the marine energy sector., Tech. rep., Marine Energy in Far Peripheral and Island Communities (MERiFIC) (February 2013 2013).

[2] R. McCall, A. Saunders, P. Shepperd, R. Beadle, Tidal power in the uk - research report 1: Uk tidal resource assessment, Tech. rep., Sustainable Development Commission (2007).

[3] D. Liang, J. Xia, R. A. Falconer, J. Zhang, Study on tidal resonance in severn estuary and bristol channel, Coastal Engineering Journal 56 (01) (2014) 1450002.

[4] J. Xia, R. a. Falconer, B. Lin, Impact of different tidal renewable energy projects on the hydrodynamic processes in the Severn Estuary, UK, Ocean Modelling 32 (1-2) (2010) 86–104. doi:10.1016/j.ocemod.2009.11.002. URL http://linkinghub.elsevier.com/retrieve/pii/S146350030900208X

[5] R. Ahmadian, R. a. Falconer, Assessment of array shape of tidal stream turbines on hydro-environmental impacts and power output, Renewable Energy 44 (2012) 318–327. doi:10.1016/j.renene.2012.01.106. URL http://linkinghub.elsevier.com/retrieve/pii/S0960148112001450

[6] D. Fallon, M. Hartnett, A. Olbert, S. Nash, The effects of array configuration on the hydro-environmental impacts of tidal turbines, Renewable Energy 64 (0) (2014) 10 – 25. doi:http://dx.doi.org/10.1016/j.renene.2013.10.035. URL http://www.sciencedirect.com/science/article/pii/S0960148113005661

[7] P. F. Cummins, The extractable power from a split tidal channel: An equivalent circuit analysis, Renewable Energy 50 (2013) 395–401.

[8] B. L. Polagye, P. C. Malte, Far-field dynamics of tidal energy extraction in channel networks, Renewable energy 36 (1) (2011) 222–234.

[9] R. Rainey, The optimum position for a tidal power barrage in the severn estuary, Journal of Fluid Mechanics 636 (2009) 497–507.

[10] I. Bryden, S. Couch, A. Owen, G. Melville, Tidal current resource assessment, Proceedings of the Institution of Mechanical Engineers, Part A: Journal of Power and Energy 221 (2) (2007) 125–135.

[11] S. Hunt, K. R. Bryan, J. C. Mullarney, The influence of wind and waves on the existence of stable intertidal morphology in meso-tidal estuaries, Geomorphology 228 (2015) 158–174.

[12] V. P. Chua, M. Xu, Impacts of sea-level rise on estuarine circulation: An idealized estuary and san francisco bay, Journal of Marine Systems 139 (2014) 58–67.

[13] J. Maskell, K. Horsburgh, M. Lewis, P. Bates, Investigating river-surge interaction in idealised estuaries, Journal of Coastal Research 30 (2) (2013) 248–259.

[14] Y. Chen, B. Lin, J. Lin, Modelling tidal current energy extraction in large area using a three-dimensional estuary model, Computers & Geosciences 72 (2014) 76–83.

[15] Z. Yang, T. Wang, Modeling the effects of tidal energy extraction on estuarine hydrodynamics in a stratified estuary, Estuaries and Coasts (2013) 1–16.

[16] S. Draper, Tidal stream energy extraction in coastal basins, PHD Dissertation, University of Oxford, Oxford, UK,.

[17] ABPmer, Atlas of UK Marine Renewable Energy Resources, http://www.renewables-atlas.info/, [Online; accessed 29-July-2015] (2015).

[18] E. Agency, DEFRA, The Estuary Guide, http://www.estuary-guide.net/, [Online; accessed 29-July-2015] (2015).

[19] N. W. C. Group, North west england and north wales shoreline management plan smp2, Halcrow Group Ltd, Swindon, UK.

[20] R. Flather, N. Heaps, Tidal computations for morecambe bay, Geophysical Journal International 42 (2) (1975) 489–517.

[21] J. N. Aldridge, Hydrodynamic model predictions of tidal asymmetry and observed sediment transport paths in morecambe bay, Estuarine, Coastal and Shelf Science 44 (1) (1997) 39–56.

[22] J. Ridgway, E. Bee, N. Breward, M. Cave, S. Chenery, C. Gowing, I. Harrison, E. Hodgkinson, B. Humphreys, M. Ingham, et al., The Mersey Estuary: sediment geochemistry, British Geological Survey, 2012.

[23] B. Hofschreuder, Flood protection and marine power in the wash estuary, united kingdom: Technical and economical feasibility study, Ph.D. thesis, TU Delft, Delft University of Technology (2012).

[24] Y. Wu, R. Falconer, R. Uncles, Modelling of water flows and cohesive sediment fluxes in the humber estuary, uk, Marine Pollution Bulletin 37 (3) (1999) 182–189.

[25] M. J. Attrill, A rehabilitated estuarine ecosystem: The environment and ecology of the Thames estuary, Springer Science & Business Media, 1998.

[26] G. Scott, A numerical study of the interaction of tidal oscillations and non-linearities in an estuary, Estuarine, Coastal and Shelf Science 39 (5) (1994) 477–496.

[27] A. Lane, D. Prandle, Changing flood risks in estuaries due to global climate change: forecasts from observations, theory and models, International Journal of Applied Mathematics and Engineering Sciences 1 (1) (2007) 69–88.

[28] M. Villars, G. Delvigne, Estuarine processes, Litterature review. Final draft prepared for CEFIC. WL. Delft hydraulics Z 2725.

[29] D. Prandle, Vulnerability of estuaries to sea level rise stage 1: a review, Tech. Rep. SC080016, Environment Agency (2010).

[30] D. Hydraulics, Mike 21 flow model fm hydrodynamic module user guide, Denmark: DHI Water Environment.

[31] D. Hydraulics, Mike 21 mike 3 flow model hydrodynamic module scientific documentation, Denmark: DHI Water & Environment.

[32] M. G. Gebreslassie, G. R. Tabor, M. R. Belmont, Numerical simulation of a new type of cross flow tidal turbine using OpenFOAM Part II: Investigation of turbine-to-turbine interaction, Renewable Energy 50 (2013) 1005–1013. doi:10.1016/j.renene.2012.08.064. URL http://linkinghub.elsevier.com/retrieve/pii/S0960148112005344

[33] M. G. Gebreslassie, G. R. Tabor, M. R. Belmont, Investigation of the performance of a staggered configuration

of tidal turbines using cfd, Renewable Energy 80 (2015) 690–698.

[34] P. Bachant, M. Wosnik, Performance measurements of cylindrical-and spherical-helical cross-flow marine hydrokinetic turbines, with estimates of exergy efficiency, Renewable Energy 74 (2015) 318–325.